Journal of Volcanology and Geothermal Research 333–334 (2017) 134–144

Contents lists available at ScienceDirect

Journal of Volcanology and Geothermal Research

journal homepage: www.elsevier.com/locate/jvolgeores

Methods for mapping and monitoring global glaciovolcanism

Aaron Curtis *, Philip Kyle

Department of Earth and Environmental Science, New Mexico Institute of Mining and Technology, Socorro, NM, USA

ARTICLE INFO

Article history:
Received 12 September 2016
Received in revised form 12 January 2017
Accepted 19 January 2017
Available online 24 January 2017

Keywords:
Glaciovolcanism
Remote sensing
Cryosphere
Volcanoes

ABSTRACT

The most deadly (Nevado del Ruiz, 1985) and the most costly (Eyjafjallajökull, 2010) eruptions of the last 100 years were both glaciovolcanic. Considering its great importance to studies of volcanic hazards, global climate, and even astrobiology, the global distribution of glaciovolcanism is insufficiently understood. We present and assess three algorithms for mapping, monitoring, and predicting likely centers of glaciovolcanic activity worldwide. Each algorithm intersects buffer zones representing known Holocene-active volcanic centers with existing datasets of snow, ice, and permafrost. Two detection algorithms, RGGA and PZGA, are simple spatial join operations computed from the Randolph Glacier Inventory and the Permafrost Zonation Index, respectively. The third, MDGA, is an algorithm run on all 15 available years of the MOD10A2 weekly snow cover product from the Terra MODIS satellite radiometer. Shortcomings and advantages of the three methods are discussed, including previously unreported blunders in the MOD10A2 dataset. Comparison of the results leads to an effective approach for integrating the three methods. We show that 20.4% of known Holocene volcanic centers host glaciers or areas of permanent snow. A further 10.9% potentially interact with permafrost.

MDGA and PZGA do not rely on any human input, rendering them useful for investigations of change over time. An intermediate step in MDGA involves estimating the snow-covered area at every Holocene volcanic center. These estimations can be updated weekly with no human intervention. To investigate the feasibility of an automatic ice-loss alert system, we consider three examples of glaciovolcanism in the MDGA weekly dataset. We also discuss the potential use of PZGA to model past and future glaciovolcanism based on global circulation model outputs. Combined, the three algorithms provide an automated system for understanding the geographic and temporal patterns of global glaciovolcanism which should be of use for hazard assessment, the search for extreme microbiomes, climate models, and implementation of ice-cover-based volcano monitoring systems.

1. Introduction

When volcanic systems interact with the cryosphere, a host of significant outcomes result. Human communities become threatened by phreatomagmatic eruptions, lahars (volcanic mud flows), jökulhlaups (glacial outburst floods), and a range of other hazards (Major and Newhall, 1989). A glaciovolcanic lahar from Nevado del Ruiz volcano killed 23,000 in 1985 (Pierson et al., 1990), and phreatomagmatic plumes from Eyjafjallajökull led to flight cancellations costing airlines as much as 3.3 billion euros (Mazzocchi et al., 2010). Glaciovolcanic processes leave a distinctive geological record containing paleoclimate information (Edwards et al., 2010). Volcanic degassing beneath thin ice also produces a unique set of ephemeral ice landforms, which can support unusual microbiomes (Connell and Staudigel, 2013; Tebo et al., 2015; Soo et al., 2009). Thus, glaciovolcanism provides a library of information, but also presents a danger. To access the former and mitigate the latter, we must learn its global distribution and extent on our planet, and begin to address how that distribution changes over time.

Glaciovolcanism, in the broad sense, includes any process whereby volcanic and geothermal systems contact four types of ice masses: snowfields, glaciers, ice sheets, and permafrost (Smellie and Edwards, 2016). Direct human access to locations of glaciovolcanism is logistically difficult and hazardous, leading to the obscurity of certain important phenomena. Warm gasses leaking from flanks and summits of snow and ice-clad volcanoes can form fumarolic ice caves, fumarolic ice towers, and ice subsidence cauldrons. Such features are rarely studied, but examples at Erebus (Curtis and Kyle, 2011; Curtis, 2015), Melbourne (Keys et al., 1983), Hood, Rainier (Zimbelman et al., 2000), Wrangell, and Baker (Kiver, 1978) suggest such modes of glaciovolcanism may be globally widespread, but largely undiscovered or unreported, leading to apparent rarity. Necessarily sparse, "boots on the ground" investigations of these often ephemeral phenomena should be complemented and targeted using worldwide assessments of glaciovolcanism.

In recent years, rich datasets regarding the distribution of the above four ice types on Earth have become available. The MODIS instrument aboard NASA's Terra satellite provides a record of weekly (8-day) global

* Corresponding author.
E-mail address: mail@aaroncurt.is (A. Curtis).

http://dx.doi.org/10.1016/j.jvolgeores.2017.01.017
0377-0273/

snow cover at 500 m spatial resolution extending back to 2000: the MOD10A2 product (Hall et al., 2006). The Randolph Glacier Inventory (RGI), a "globally complete" catalog of glaciers, was compiled by Pfeffer et al. (2014). Ice within the soil is more difficult to map; it is not observable by remote sensing alone. Using elevation data and global air temperature data from general circulation models (GCM), Gruber (2012) was able to create a high-resolution model called the Permafrost Zonation Index (PZI) which provides an estimate of frozen ground extent worldwide. In the Northern Hemisphere, PZI closely matches the commonly used Circum-Arctic Map of Permafrost and Ground-Ice Conditions (Brown et al., 1997), and it was validated for use in the Himalayas by Schmid et al. (2015) and in New Zealand by Sattler et al. (2016). Many decades of field investigation provide good constraints on the locations of volcanic centers active during the Holocene. The best catalog is the Smithsonian Institution's Volcanoes of the World (VOTW) database, which contains entries for 1443 terrestrial volcanoes (and 113 seamounts) (Global Volcanism Program, 2013).

Before these datasets were available, no global map of glaciovolcanism existed, although compilations of case studies such as Major and Newhall (1989) did exist. Curtis (2014) produced a preliminary global map using MOD10A2 data. In 2015 and 2016, worldwide maps were published, but lacked description of the methods used to create them. Fig. 1 of Waitt et al. (2015) cites the use of GLIMS (Global Land Ice Measurements from Space) polygon data, but displays ice-clad volcanoes in areas (e.g. Aleutian Islands) where no GLIMS polygons exist. Presumably, the spatial analysis was manually augmented based on expert knowledge. Smellie and Edwards (2016) include similar maps, but they must be considered illustrative schematics rather than quantitative global surveys as they are presented without a description of input data or cartographic methods. In an effort to produce a systematic global survey, we present and evaluate three glaciovolcanic potential detection algorithms (MDGA, RGGA, PZGA) of potential glaciovolcanism, using the aforementioned global geospatial datasets (MOD10A2, RGI, PZI, VOTW) as input.

In the course of developing methods for observing global glaciovolcanism spatially, we assess to what extent these tools are also useful for volcano monitoring. Several near-real-time volcano monitoring and eruption alert systems are already in operation, based on remote sensing of thermal and gas concentration anomalies. The MODVOLC system leverages thermal sensing to detect molten lava, based on data from the MODIS instrument (which we are also using here for the MDGA system) (Wright et al., 2015). SACS combines data from several satellites to provide automated alerts of SO_2 plumes (Brenot et al., 2014). However, there no system has been developed to detect the loss of ice mass and area associated with glaciovolcanism. Such ice loss was the first observable precursor of the Redoubt eruption in 2009 (Bleick et al., 2013). An autonomous, satellite-based system to detect ice loss induced by volcanic activity would provide an important complement to existing thermal and gas monitoring capabilities.

2. Background

Chapman et al. (2000) provided a useful classification of glaciovolcanism, dividing it into three types: (1) volcanic interaction with snow, firn, and thin ice masses, generally <100 m, (2) volcanic interaction with thick, extensive glaciers and ice sheets, and (3) volcanic interaction with permafrost. Although Chapman et al. primarily referred to eruptions, we combine these categories with a broader definition of glaciovolcanism: processes resulting from interaction between any volcanic emissions (including flank degassing and emissions from hydrothermal systems) and nearby ice. Smellie and Edwards (2016, Ch. 2) provide a regionally grouped review of known glaciovolcanic centers across all three types based on existing literature, extending deeper into geological time than the current Holocene-focused work.

Type 2 glaciovolcanism produces the most recognizable deposits (tuyas, tindars, and associated lithofacies), and are best represented in the literature. Many studied Type 2 deposits date to the Last Glacial Maximum. Type 1 is common at alpine volcanoes but is only rarely recognizable in the geological record. Tuffen and Castro (2009) described the first discovery of an eruption deposit demonstrably formed beneath "thin" ice, "only 35–55 m thick." Eruption into such snowpacks at Fimmvörðuháls and Tolbachick were recently observed in situ by Edwards et al. (2012, 2014). Alpine firn fields and thin glaciers respond not only to eruption of lava, but also undergo significant melting and deformation in response to fumarolic activity and flank degassing. Loss of alpine ice masses in response to increased degassing can be an early indicator of volcanic unrest (Bleick et al., 2013; Kiver, 1978). In some arid environments, galciovolcanism is the only process capable of supplying water to biological communities and for aqueous mineral processes such as weathering. This primarily occurs at Type 1 systems like Mt. Erebus, Antarctica, where fumarolic degassing not only produces liquid water but also melts caves into the summit caldera ice mass. Native microbiological ecosystems with unusual metabolic strategies and molecular machinery have recently been identified in the caves (Connell and Staudigel, 2013; Tebo et al., 2015). Firn caves in the summit crater of Mount Rainier are also likely to host a microbiome. "Warm ground" areas occur when volcanic heating melts holes in the ice cover, supporting patches of moss in the otherwise inhospitable Antarctic (Broady et al., 1987; Soo et al., 2009). These ecosystems depend on the water, consistently warm microclimate, and UV protection in the case of caves, all of which are available due to glaciovolcanism.

The remaining category of glaciovolcanic processes, Type 3, occurs when magma bodies and related hydrothermal and volcanic systems encounter permafrost. This may be the primary glaciovolcanic phenomenon in the geologic history of Mars, where the major water reservoir is known as the cryolithosphere, a permafrost-like layer which is thought to be more than 9 km deep for the majority of the planet (Head and Wilson, 2007). On Earth, Type 3 is particularly well studied in Kamchatka (Abramov et al., 2008).

It is becoming increasingly clear that interactions between the global cryosphere and magma bodies play a role in global climate. Huybers and Langmuir (2009) observed an increase in eruption rate during the last deglaciation and suggested depressurization of magma chambers by the removal of ice overburden as a causative factor. Recent work on submarine volcanism supports this type of process. Midocean ridge eruption frequency appears to increase in response to depressurization from falling sea levels (Conrad, 2015; Tolstoy, 2015). Mapping the distribution of glaciovolcanism is an important precursor to global models of the type of feedback between glaciation and subaerial volcanism.

3. Methods

We created three detection algorithms for locations of glaciovolcanic potential (Fig. 1) by intersecting circular buffers of 10 km diameter drawn around each VOTW volcano coordinate with a satellite snow cover product (MOD10A2), a global inventory of glaciers (RGI), and a global permafrost model (PZI). Most VOTW coordinates correspond to stratovolcano summit locations. VOTW coordinates representing volcanic fields, such as clusters of cinder cones, are generally located near the centroid of the cluster. Large caldera complexes are notable exceptions and glaciovolcanism in those locations may be poorly represented in this study. If a database representing volcanic centers as polygons rather than points becomes available, it could be incorporated into the present work to remove this issue. This buffer zone also accounts for the various errors which VOTW warns is inherent in their coordinates (Smithsonian Institution, 2013).

The MOD10A2 product is computed using a "normalized difference snow index" (NDSI) based on the difference between MODIS bands 4 (0.55 μm) and 6 (1.6 μm). A set of algorithms centered on NDSI are used to classify each pixel as one of several ground cover types including "snow," "cloud," "land," and "lake ice" (Hall et al., 2006). Multiple values obtained during the 8-day period are combined, and if a pixel (roughly

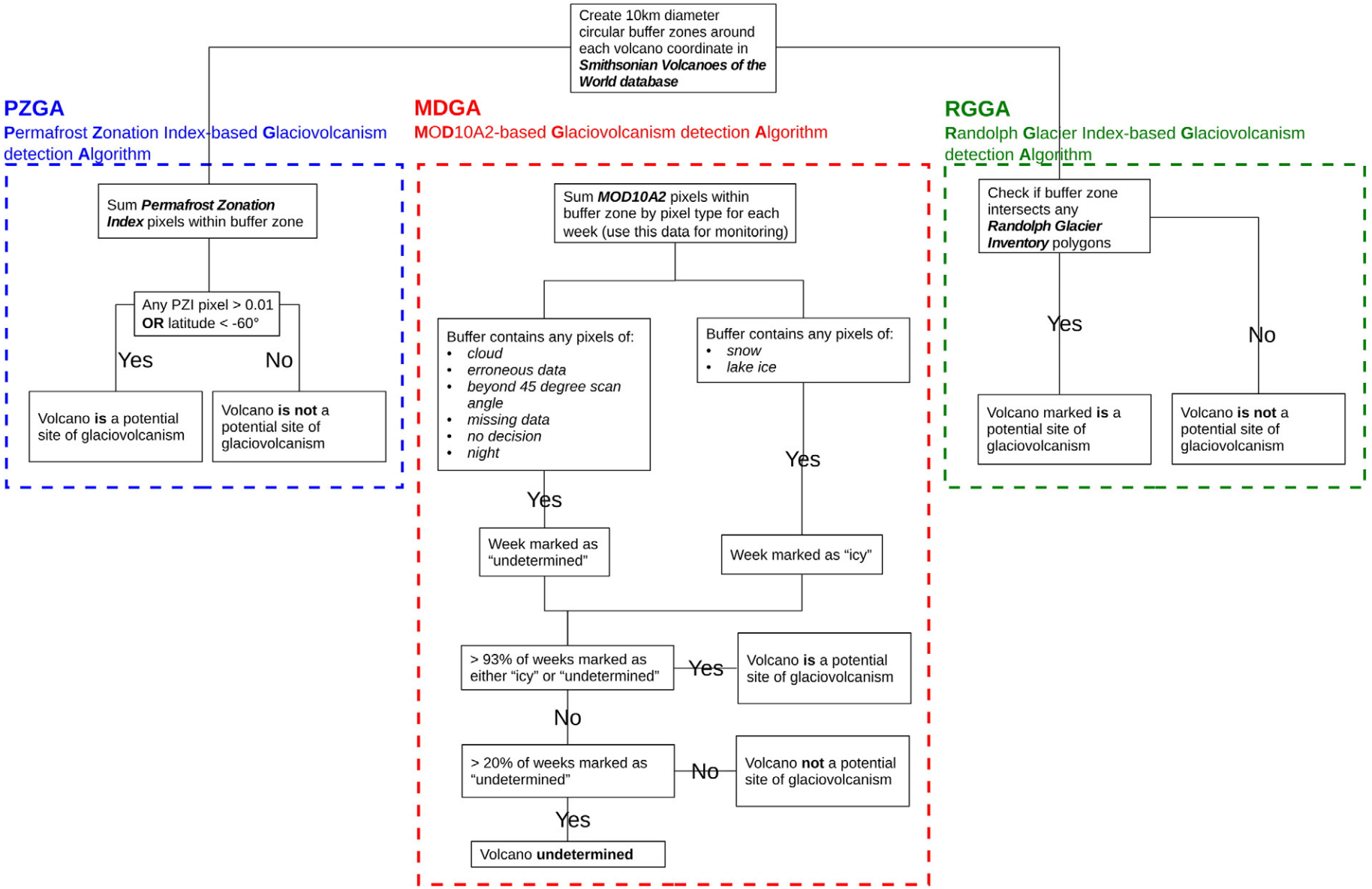

Fig. 1. Algorithms used in this paper to detect locations of potential Holocene volcano-ice interaction. Input datasets are in boldface italics, and algorithm output is in boldface.

500 × 500 m) is detected to be snowy in any of the measurements, the reported value will be "snow" for that week. In this way, MOD10A2 reduces the impact of obstructing factors – primarily clouds. To create MDGA, we calculated pixel sums for each ground cover type within each volcano buffer zone for each week of data. A total of 711 weeks (from Feburary 26, 2000 to August 13, 2015) were processed. MDGA classifies each volcano as "icy," "not icy," or "undetermined" using a heuristic we designed to account for cloud cover and other imperfections in the dataset, which requires 93% of weeks to be marked icy or undetermined, and <20% marked as undetermined (Fig. 1).

Cloud cover presents the most serious deficiency in the MOD10A2 data, leading to the majority of "undetermined" MDGA results. Where cloud does not obscure the measurement, Hall and Riggs (2007) found MOD10A2 to be around 93% accurate when compared to ground truthing and other snow cover products. Known flaws include non-detection of thin snow and occasional misclassification between snow and clouds. We found blunders in the data that had not been reported in previous studies including the frequent detection of "lake ice" at the summits of stratovolcanoes, and one week in which large portions of Antarctica were reported to be ice-free ground (Fig. 2). The MOD10A2 User Guide does acknowledge "Snow mapping and lake ice mapping errors" due to ambiguous values of NDSI, but states they are "commonly in the ≤0.001 percentage range of pixels" (Riggs et al., 2006, p. 15). Unfortunately, MOD10A2 lacks coverage of the polar regions during local winter, because MODIS is a passive radiometer, measuring reflected sunlight. Fig. 3 shows the total pixel count for the most southerly and northerly volcanoes in VOTW.

The erroneous "lake ice" pixels are a persistent pattern at many volcanoes, comprising several percent of the data (Table 1). Correcting these pixels is complicated by the fact that lake ice actually exists within the buffer zone of some of these volcanoes. However, the buffer zones for Rainier, Etna, Adams, Baker, and Fujisan contain no lakes, despite the fact that more than 1% of the data reports lake ice. To deal with this situation, lake ice pixels were treated as snow in the MDGA algorithm (Fig. 1).

Like MOD10A2, the permafrost zonation index (PZI) is a raster dataset. It is calculated at 1 km global resolution with input data from air temperature models (NCAR-NCEP and CRU TS 1.0) and global terrain elevation data. It extends to the North Pole, and to 60°S, beyond which insufficient model input data is available, but permafrost coverage is assumed to be regionally complete. PZI values are given from 0 (no permafrost exists in this pixel) to 1 (continuous permafrost fills all environments in this pixel) with the recognition that ground temperatures are extremely heterogenous at the sub-pixel scale (Gruber, 2012).

Unlike PZI and MOD10A2, RGI is a vector dataset. It consists of polygons that represent the boundaries of known glaciers compiled by experts with the use of a wide range of data sources including fieldwork and satellite remote sensing. RGI has become iteratively more comprehensive as more glaciers are contributed, and now claims to be "globally complete," a contention which we discuss when comparing output derived from it to our two other glaciovolcanism detection methods. RGI is strictly a dataset of glaciers, and does not contain polygons for ice sheets. Therefore, we supplemented RGI with ice sheet polygons from OpenStreetMap (Topf and Hormann, 2015). To create RGGA, we

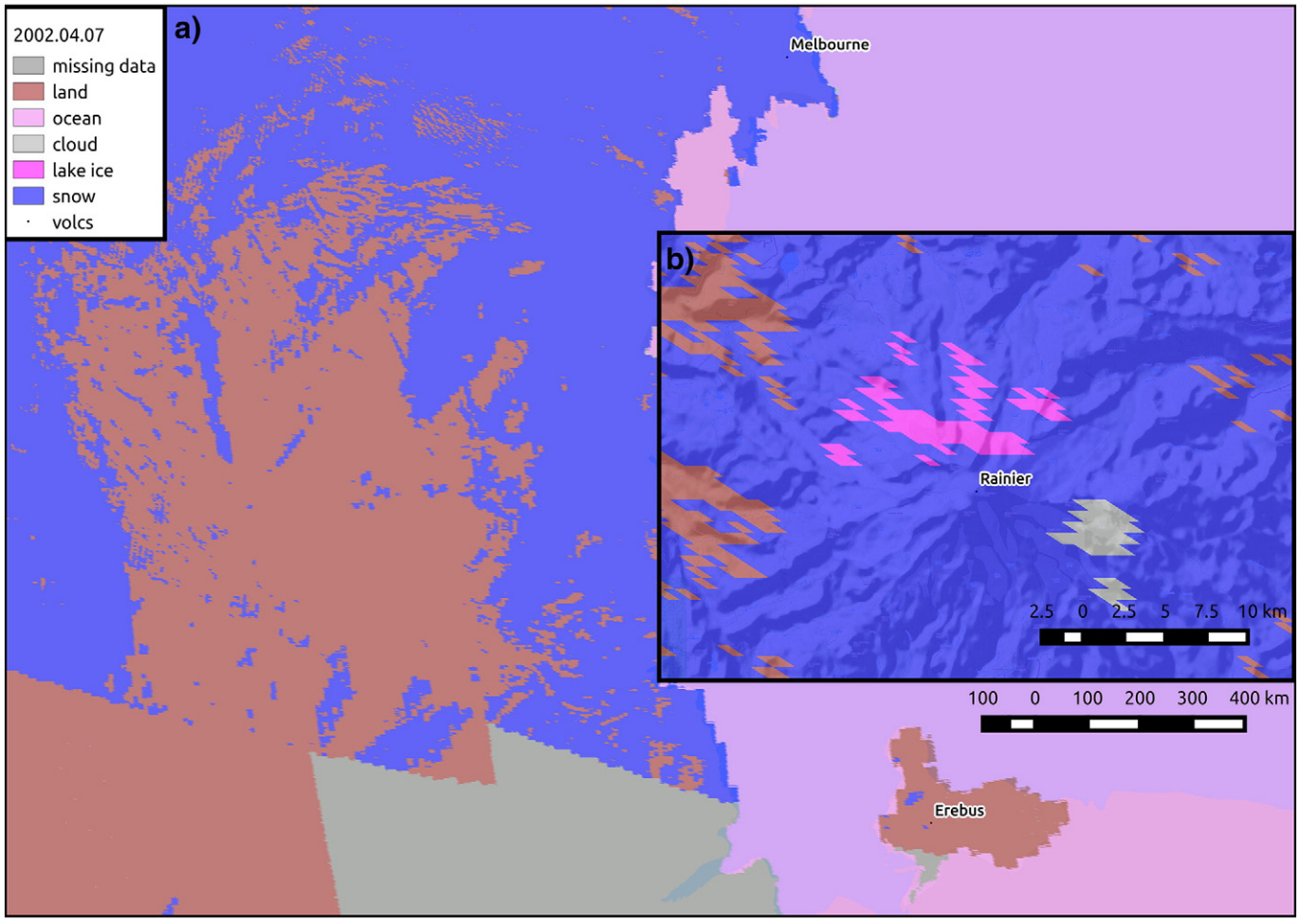

Fig. 2. Previously unreported blunders in MOD10A2, shown for April 7, 2002. a) Bare ground covers much of Ross Island and Victoria land. b) Snow on certain volcanoes is often misclassified as "lake ice." Although only one week of data is shown here, the problem persists at Mt. Rainier throughout the dataset.

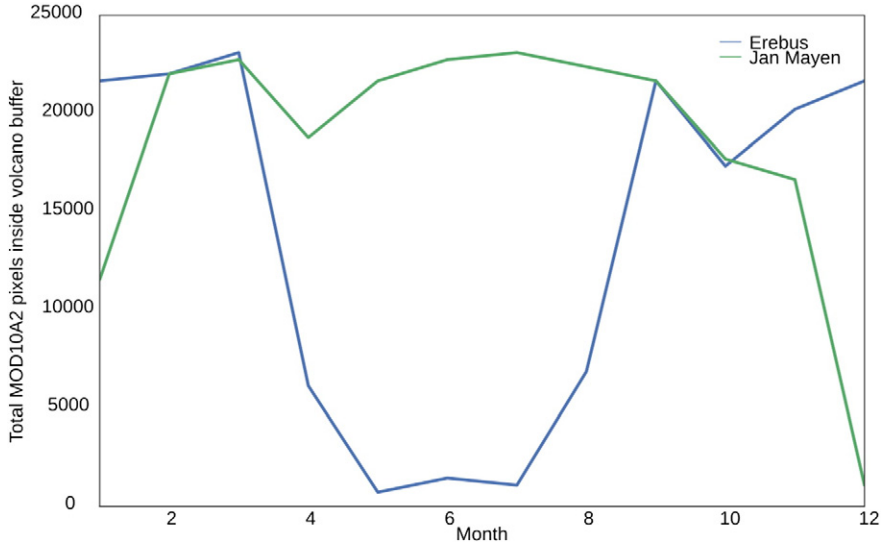

Fig. 3. Availability of MOD10A2 data for the world's most northern and southern Holocene volcanoes is poor during local winter because of low insolation.

calculated polygon intersections between volcano buffer zones and glacier/ice sheet polygons.

4. Results

A total of 451 terrestrial volcanoes (31.3%) were determined to be potential sites of Holocene and present glaciovolcanism by at least one of the three algorithms (MDGA, RGGA, and PZGA). Of those, 139 (9.6%) triggered all three algorithms. Most (153) detections by MDGA (193 total) and RGGA (254 total) triggered both of those algorithms. PZGA detected far more volcanoes than MDGA or RGGA, at 403. A full listing of detections is given in Table S1, and totals are shown in Table 2.

Geographically, the highest concentrations of PZGA-only detections were in southern Kamchatka (Fig. 4d) and in Japan. This is expected given local meteorological conditions, which are periglacial rather than glacial. The mean annual air temperature in the mountains at these locations is near zero, allowing for the formation of discontinuous permafrost but insufficient for the preservation of snow and ice above ground.

In addition to counts and geographical distributions of glaciovolcanism, MDGA can provide some information about glaciovolcanism over time. The input to the RGGA and PZGA algorithms are datasets in which the dimension of time has already been aggregated. MDGA, however, calculates area statistics for all 771 weeks to look for volcanoes that always have an area of snow. Weekly area statistics provide an instructive intermediate data product (Fig. 5). MDGA weekly ground cover area data can also be used to contrast eruptive periods with the seasonal baseline snow cover patterns. There are tens of glaciovolcanic events in the MDGA weekly dataset, and we have selected three for a detailed analysis: the 2005–2006 eruption of Augustine, the 2008–2009 eruption of Redoubt, and the 2015 eruption of Cotopaxi (Fig. 6). We selected these due to low cloud cover and because they are locations where Type 1 activity initiated after many years of quiescence.

At Augustine volcano, Alaska, in 2005, precursory earthquake swarms beginning in May and phreatic explosions in December led to a magmatic explosive phase with plumes up to 9 km high (Wallace et al., 2010). Augustine does not host glaciers, but our data shows it hosts snow nearly year-round, with a baseline pattern which is only snow-free in July. A sudden sixfold increase in observed cloudy pixels (Fig. 6a) corresponds to the first steam plume of the eruption on December 12, 2005 (Bailey et al., 2010). Cloudy pixel count returned to the seasonal background levels in March, at the end of the eruption. There appears to be a significant drop in snow cover, of around 50 MODIS pixels (12.5 km^2), in early 2006. A ~ 70 MODIS pixel (17.5 km^2) increase in observed ice-free land area beginning in early January 2006 roughly matches the reported area of lava flows and dome growth as reported by Wallace et al. (2010). The subsequent reduction in land area likely represents accumulation of snowfall, gradually burying the freshly emplaced lava. The return of snow cover in February 2006 can be corroborated by comparing aerial images B and C in Fig. 6 of van Manen et al. (2010).

Mt Redoubt hosts a far larger and more permanent ice volume than Augustine, with glaciers measured as thick as 180 m (Trabant and Hawkins, 1997). In Summer 2008, Redoubt displayed subtle unrest observed after the fact in geodetic data as inflation (Grapenthin et al., 2013) and localized snow and ice melting (Bleick et al., 2013). Between March 15 and April 4, the eruption progressed through an explosive phase including 19 explosions with plume heights up to 18.9 km, pyroclastic density currents and lahars summing to ~79 to 120 M m^3 dense rock equivalent. An effusive dome-building phase continued until July 1.

The MDGA weekly dataset for Redoubt surrounding the 2009 eruptive phase appears to show eruptive and plumes and the results of

Table 1
Volcanoes with the most lake ice pixels reported in MOD10A2, shown as percentage of all data for 2000 through 2015.

Kurile Lake	20.1%	Eyjafjallajökull	3.9%	Ilyinsky	2.3%
Taryatu-Chulutu	16.2%	Crater Lake	3.7%	Krafla	2.2%
Craters of the Moon	9.8%	Atlin Volcanic Field	3.4%	Baker	2.2%
Askja	8.9%	Unnamed	2.6%	Ingakslugwat Hills	2.1%
Etna	7.1%	Newberry	2.5%	Akademia Nauk	1.8%
Rainier	6.4%	Sanford	2.5%	Fujisan	1.7%
Adams	5.3%	Yellowstone	2.5%	Tao-Rusyr Caldera	1.6%
Garibaldi Lake	4.9%	Mono Lake Volcanic Field	2.4%	Snaefellsjökull	1.6%

Table 2
Counts of detected potential volcano-ice interaction centers active in the Holocene for MDGA, RGGA, and PZGA, with percents out of the 1443 subaerial volcanoes in the GVP. Where different detection algorithms are present in the table row and column, the corresponding cell represents the number of volcano-ice interaction centers detected by both. A total of 451 volcanoes (31.3%) were marked as potential sites of glaciovolcanism by at least one algorithm.

	MDGA	RGGA	PZGA
PZGA	166 (11.5%)	219 (15.2%)	403 (27.9%)
RGGA	153 (10.6%)	254 (17.6%)	
MDGA	193 (13.4%)		

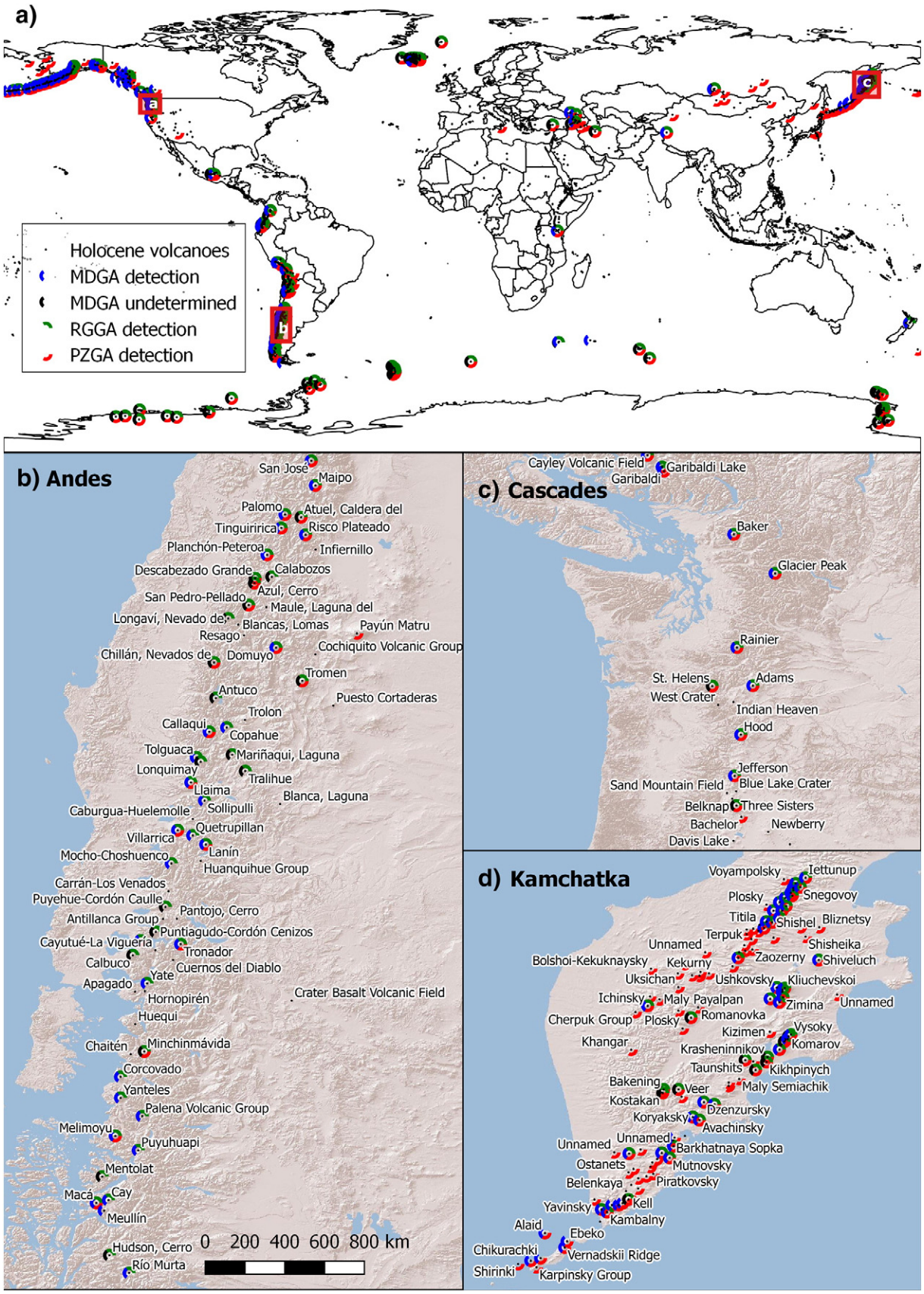

Fig. 4. Locations of likely glaciovolcanism detected using the three methods developed here in volcanically active regions. Blue and green wedges (MDGA and RGGA) are indications of potential Type 1 (eruption beneath ice sheet or major glacier) or 2 (volcanic activity beneath alpine snow) potential. Red wedges (PZGA) indicate Type 3 potential (volcanic interaction with permafrost). Scalebar in b) also applies to c) and d).

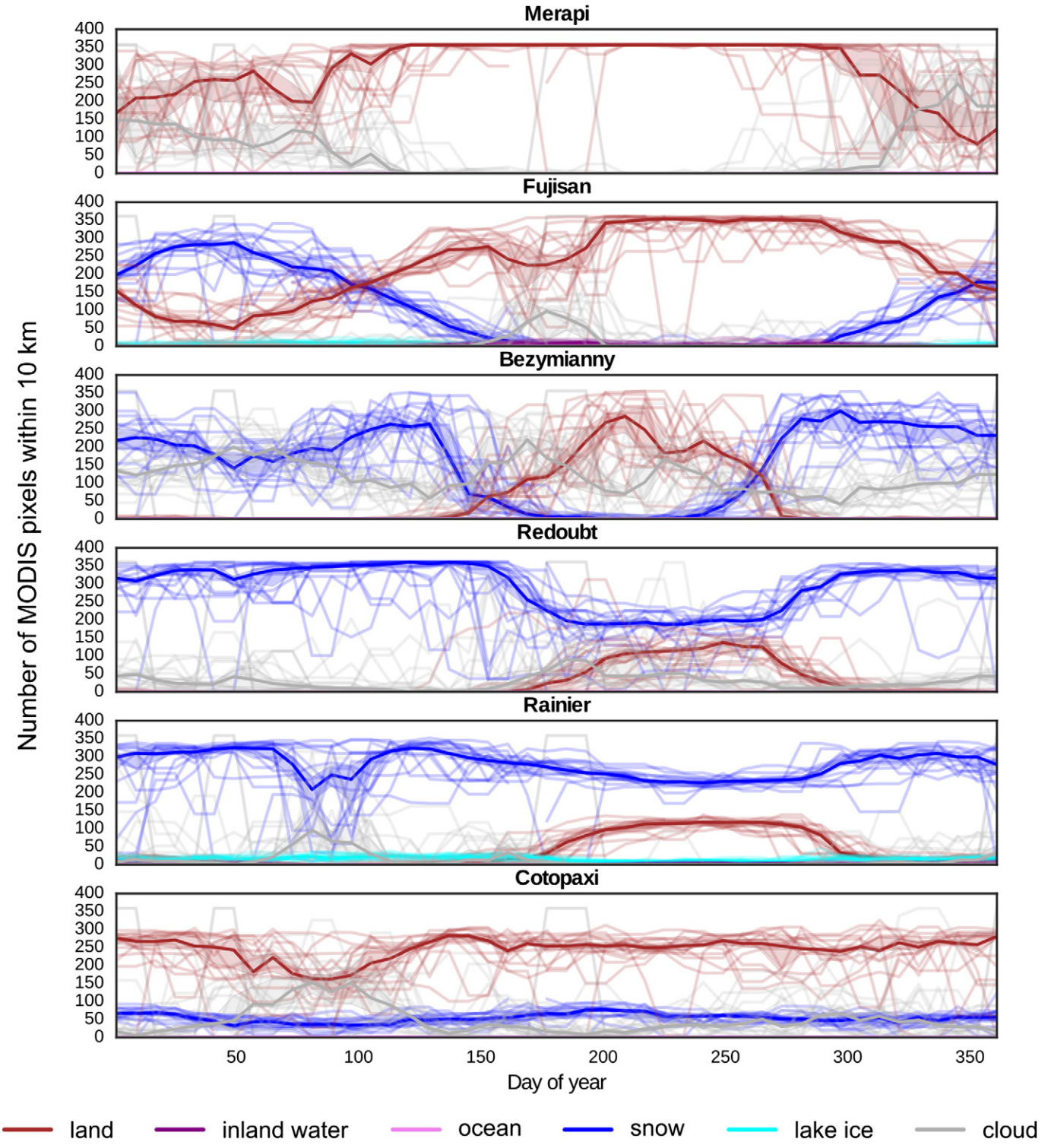

Fig. 5. MOD10A2 pixel values within 10 km buffer zones surrounding selected volcanoes. Data is shown for 2000 through 2015, with each year shown as one light-colored line on the plot. The median is shown as a darker line, and the 68% bootstrap confidence interval is shaded.

ashfall (Fig. 6b). A "cloud" peak of ~200 MODIS pixels (~50 km^2) begins in March. Ash and snow deposits were interleaved during the eruptive period, and a period of high incident solar radiation in late May led to snowmelt and the exposure of multiple layers of buried tephra, causing a sharp increase in MODIS "land" pixels of about 250 (~62.5 km^2). This is corroborated by webcam images, in which the majority of the volcano suddenly appears dark in color despite its thick glacial mantle. Ice loss from pre-eruptive melting is not obvious in the dataset, and is probably too small to be evident. The largest of the several "holes in the ice" reported by Bleick et al. (2013) was only 0.08 km^2, which would be less than one MODIS pixel.

In terms of ice mass, Cotopaxi lies somewhere between Augustine and Redoubt. Its upper 1000 m is permanently ice-capped, hosting 15 km^2 of glaciers. The 2015 eruption began on 15 August, with a 12 to 13 km ash plume. Eruptions continued with plumes of decreasing altitude until 24 Jan 2016. During this time the evidence of glacial melting

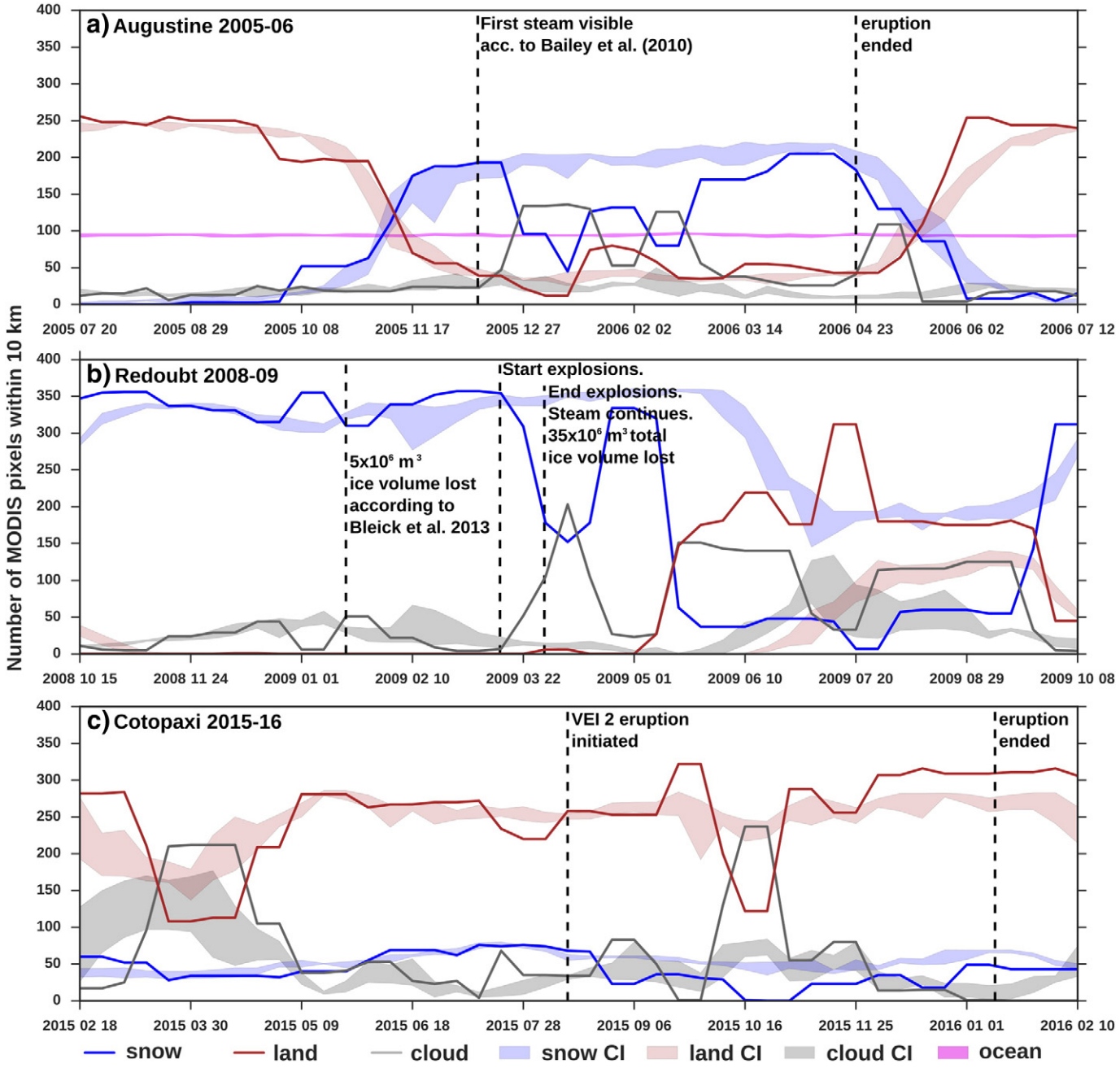

Fig. 6. Snow cover within MDGA buffer for three selected glaciovolcanic eruptions compared with background annual pattern. Filled areas are 68% bootstrap confidence interval of the median for 2000 through 2015. Plumes, ashfall, and ice mass loss contribute to the discrepancy between the solid lines and filled areas of the corresponding land cover classification.

was constant: new meltwater streams issued from the glaciers and large, visible cracks opened (Global Volcanism Program, 2016). A comparison between Cotopaxi orthophotos taken by Ramon et al. (2016) revealed 0.49 km^2 ice loss between 18 August 2015 and 8 October 2015. Unfortunately, detailed ice loss information is not available during the later stages of the eruption, which persisted through November. In Fig. 6c ice loss, and "land" gain, begins around the initiation of the eruption sequence and appears to affect between 10 and 30 MODIS pixels (2.5 km^2 to 7.5 km^2). Although cloud or plume obstructs the data in October, the signal is fairly constant over several months.

5. Discussion

To what extent do these three algorithms, derived from independent datasets of global iciness, represent the same conditions? To investigate consistency and redundancy, we conducted a Cohen's κ analysis to assess agreement between the three algorithms (Table 3). κ is 0 when computed between a pair of random variables, 1.0 between variables which agree perfectly, and −1.0 between variables which differ on all observations. Using the Landis and Koch (1977) classification of κ values, comparison between RGGA and MDGA shows "Substantial agreement," while the κ between PZGA and the other two algorithms indicates "Moderate agreement."

Table 3
Cohen's κ statistic for pairs of glaciovolcanism detection algorithms.

	MDGA	RGGA
PZGA	0.46	0.57
RGGA	0.63	

Indeed, we would not expect PZGA to be equivalent to MDGA and RGGA, because it is testing for interaction with frozen ground rather than above-ground ice (Type 3 glaciovolcanism, which we might call "periglaciovolcanism"). Differences between MDGA and RGGA are primarily due to the fact that permanent snow may exist without forming a glacier. The majority of the 40 volcanic centers identified as locations of potential glaciovolcanism by MDGA but not RGGA are areas with small patches of permanent snow, such as Chikurachki volcano in the Kurile Islands and Augustine in Alaska. These snowfields have not reached the thickness, about 30 m, required to initiate the plastic flow required for them to be designated glaciers (Paterson, 1994). In fact, the difference between MDGA and RGGA results could actually be used to determine locations of volcano interaction with thin ice masses (Type 2). In constructing a global map of glaciovolcanism, we feel it is most appropriate to combine MDGA and RGGA detections as indicating Type 1 and Type 2 glaciovolcanism but consider PZGA-only detections as indicating Type 3.

Some of the RGGA non-detections are due to shortcomings in the expert-compiled RGI dataset. While RGI 5.0 claims to be globally complete, some Aleutian summit crater glaciers are missing. RGI contains no glacier polygons on Tanaga Island, Alaska, but the USGS hazard assessment states that one of the craters on the island's Takawangha summit is "covered partly by glacial ice" (Coombs et al., 2007). The same is true for nearby Gareloi (Coombs et al., 2008). In both cases, the hazard assessment states that lahars would likely result from glaciovolcanism in case of eruption. Given this evidence, we can assume that glaciers in other remote locations, for example, in the Kurile Islands, may also be missing in this database.

MDGA's strength, as well as its greatest weakness, is that it is calculated without any human input. In compiling RGI, experts take advantage of human fieldwork on glaciers which is free from the obstruction of clouds and not restricted by satellite orbital geometry. Clouds accounted for 45.8% of the MOD10A2 data within the volcano buffers, despite the fact that the algorithm combining daily data into MOD10A2 weekly data is designed to minimize cloudy pixels. On the other hand, weekly automatic observations allow for a richer dataset that can be analyzed for seasonal and interannual variation. For example, it is evident from Fig. 5 that although both Cotopaxi and Bezymianny host snow year-round, Bezymianny has much higher seasonal variability in snow cover. This might suggest that volcano-ice interactions are significantly more of a concern at Bezymianny during the winter.

MDGA weekly data is able to detect ice mass loss due to volcanic activity in certain circumstances. It revealed volcanic melting of snowpack at Augustine in 2005–2006, which was replaced by new snow following eruptive cessation, and the loss of several km2 of glaciers on Cotopaxi in 2015. Our case study of the Redoubt 2008–2009 eruption, in contrast, highlighted potential red herrings in the MDGA weekly data. Any ice loss signal was overwhelmed by eruptive plume pixels (reported as "cloud"), and supra-glacial ash deposit pixels (reported as "land").

PZGA is also fully automated, with the added benefit that it can be easily re-run for past or future scenarios. Because PZGA is computed from mean annual air temperatures (MAAT) and topography, it could be run using output from a global circulation model. Provided that data is available for the location of volcanic centers, PZGA could be used to create global glaciovolcanism maps during previous glaciations and for the future, as global deglaciation continues. However, PZGA is not capable of detecting volcanic unrest because it relies on air temperature measurements rather than direct observation of permafrost and therefore lacks sensitivity to local volcanic heating.

6. Conclusions and implications

Glaciovolcanism is pervasive on Earth, extending from the equator to beyond the polar circles. Of the 1443 known subaerial Holocene volcanic centers, 294 (20.3%) are glaciated or have permanent snowfields and could be sites of Type 1 and/or Type 2 glaciovolcanism. A further 157 (10.9%) are close enough to areas of permafrost to allow for Type 3 glaciovolcanism. Type 1 and 2 are present in most plate-boundary and hotspot volcanic regions, with the notable exceptions of Southeast Asia and Central America. Volcanoes with exclusively Type 3 glaciovolcanism are primarily clustered in five regions: Southwest Alaska, Western Canada, the Atacama Desert, a cluster in the Caucasus, and a band extending from Mongolia to Japan and including southern Kamchatka.

Each of the three algorithms presented here has unique capabilities and shortcomings (Table 4). MDGA can be used to investigate changes in the extent of snow and ice cover at volcanoes on a weekly timescale, but it is vulnerable to errors in edge cases, and less effective in cloudy areas and high latitudes. RGGA provides the most definitive determinations, but because it relies on a dataset compiled by humans it is vulnerable to omission of glaciers in remote areas and may be updated with insufficient frequency as global glacier area changes. Like MDGA, PZGA may be processed frequently and also can be run for hypothetical climate regimes because of its minimal data requirements (global MAAT history and topography), but only detects volcano-permafrost interaction and so is less useful for evaluation of volcanic hazards. Combined, the three algorithms produce the most comprehensive view of global glaciovolcanism possible with available data.

All three depend on availability of coordinates for volcanic centers – a dataset that is necessarily incomplete as many eruptions leave cryptic or nonexistent geological records due to erosion or burial. It is likely that many volcanic deposits, even those of Holocene age, are yet to be found and cataloged. Of particular concern are deep subglacial deposits such as the roughly 1000 anomalies located in aeromagnetic surveys beneath the West Antarctic Ice Sheet which Behrendt (2013) identifies as volcanic centers. Further investigation of these anomalies is strongly recommended. However, a greater focus on observations of Type 1 glaciovolcanism – particularly interactions between stratovolcanoes

Table 4
Summary of utility of methods presented here for various applications. Mapping: Determining the global distribution of glaciovolcanism today. Monitoring: Observing changes in ice cover to detect initiation of volcanic unrest. Modeling: Predicting the global distribution of glaciovolcanism in past or future climates or on other worlds.

		Utility of methods		
	Source data	Mapping	Monitoring	Modeling
MDGA	Smithsonian Volcanoes of the World (VOTW) database and MOD10A2, the weekly 500 m snow cover product from MODIS sensor on Terra satellite	Effective for Type 1 and 2 volcano-ice interaction	Weekly data calculated in an intermediate step is capable of automatically detecting ice mass loss on volcanoes hosting thin ice masses (Type 1) where activity causes change in ice-covered area	Unsuitable; would require simulation of MODIS observations
RGGA	VOTW, Randolph Glacier Inventory (RGI) expert-compiled glacier polygons, and OpenStreetMap ice sheet data	Effective for Type 1 and 2 volcano-ice interaction	Unsuitable; would require manual updates to underlying RGI dataset	Unsuitable; would require manual updates to underlying RGI dataset
PZGA	VOTW and Permafrost Zonation Index (PZI) global permafrost model	Effective for type 3 volcano-ice interaction	Unsuitable; relies on regional air temperature measurements and cannot detect local permafrost loss from volcanic activity	Suitable; PZI dataset can be recomputed using GCM output

and their alpine ice – could enable us to mitigate major glaciovolcanism hazards.

The baseline annual snow cover pattern for each volcano we calculated from MDGA weekly data (Fig. 5) is a useful dataset for understanding seasonality of hazards. The Augustine and Cotopaxi case studies demonstrated that MDGA weekly data is also capable of detecting change in ice area under certain circumstances. However, eruptive plumes and supra-glacial ash present noise sources which can overwhelm the ice change signal, as in the Redoubt case. Future work should seek to reduce or eliminate these problems by increasing the spatial and/or temporal granularity of the input data. Rather than observing a 10 km buffer zone, a more refined glaciovolcanism monitoring system could identify individual pixels of perennial snow or glacial ice once they have been consistently observed over a sufficient time period, and watch those individual pixels for melt. Additionally, the system could be run using daily MODIS data rather than the weekly aggregate data we employ here, reducing the obstructive impact of eruption plumes. Such a system could be extremely useful and could conceivably detect remote Type 2 glaciovolcanism in advance of or in the absence of a detectable ash or SO_2 plume.

Acknowledgements

This work was funded by NSF Grant ANT1142083. Thanks to Ronni Grapenthin and Erica Emry for comments on early versions of the manuscript, and to the two anonymous reviewers.

Appendix A. Supplementary data

Supplementary data associated with this article can be found in the online version, at http://dx.doi.org/10.1016/10.1016/j.jvolgeores.2017.01.017. These data include the Google map of the most important areas described in this article.

References

Abramov, A., Gruber, S., Gilichinsky, D., 2008. Mountain permafrost on active volcanoes: field data and statistical mapping, Klyuchevskaya volcano group, Kamchatka, Russia. Permafr. Periglac. Process. 19:261–277. http://dx.doi.org/10.1002/ppp.622.

Bailey, J.E., Dean, K.G., Dehn, Jonathan, Webley, P.W., 2010. Integrated satellite observations of the 2006 eruption of Augustine Volcano, chapter 20. In: Power, J.A., Coombs, M.L., Freymueller, J.T. (Eds.), The 2006 Eruption of Augustine Volcano, Alaska: U.S. Geological Survey Professional Paper 1769:pp. 481–506 (https://pubs.usgs.gov/pp/1769/chapters/p1769_chapter20.pdf).

Behrendt, J.C., 2013. The aeromagnetic method as a tool to identify Cenozoic magmatism in the West Antarctic Rift system beneath the West Antarctic Ice Sheet — a review; Thiel subglacial volcano as possible source of the ash layer in the WAISCORE. Tectonophysics 585:124–136. http://dx.doi.org/10.1016/j.tecto.2012.06.035.

Bleick, H.A., Coombs, M.L., Cervelli, P.F., Bull, K.F., Wessels, R.L., 2013. Volcano–ice interactions precursory to the 2009 eruption of Redoubt Volcano, Alaska. J. Volcanol. Geotherm. Res. 259:373–388. http://dx.doi.org/10.1016/j.jvolgeores.2012.10.008 (The 2009 Eruption of Redoubt Volcano, Alaska).

Brenot, H., Theys, N., Clarisse, L., van Geffen, J., van Gent, J., Van Roozendael, M., van der A, R., Hurtmans, D., Coheur, P.-F., Clerbaux, C., Valks, P., Hedelt, P., Prata, F., Rasson, O., Sievers, K., Zehner, C., 2014. Support to aviation control service (SACS): an online service for near-real-time satellite monitoring of volcanic plumes. Nat. Hazards Earth Syst. Sci. 14:1099–1123. http://dx.doi.org/10.5194/nhess-14-1099-2014.

Broady, P., Given, D., Greenfield, L., Thompson, K., 1987. The biota and environment of fumaroles on Mt Melbourne, Northern Victoria Land. Polar Biol. 7, 97–113.

Brown, J., Ferrians Jr, O.J., Heginbottom, J.A., Melnikov, E.S., 1997. International Permafrost Association Circum-Arctic Map of Permafrost and Ground Ice Conditions. U.S. Geological Survey CircumPacific Map Series, Map CP45, Scale 1:10,000,000, Washington, DC, USA.

Chapman, M.G., Allen, C.C., Gudmundsson, M.T., Gulick, V.C., Jakobsson, S.P., Lucchitta, B.K., Skilling, I.P., Waitt, R.B., 2000. Volcanism and ice interactions on Earth and Mars. Environmental Effects on Volcanic Eruptions. Springer, pp. 39–73.

Connell, L., Staudigel, H., 2013. Fungal diversity in a dark oligotrophic volcanic ecosystem (DOVE) on Mount Erebus, Antarctica. Biology 2:798–809. http://dx.doi.org/10.3390/biology2020798.

Conrad, C.P., 2015. How climate influences sea-floor topography. Science 347:1204–1205. http://dx.doi.org/10.1126/science.aaa6813.

Coombs, M.L., McGimsey, R.G., Browne, B.L., 2007. Preliminary Volcano-hazard Assessment for the Tanaga Volcanic Cluster, Tanaga Island, Alaska. US Geological Survey.

Coombs, M.L., McGimsey, R.G., Browne, B.L., 2008. Preliminary Volcano-hazard Assessment for Gareloi Volcano, Gareloi Island, Alaska. US Geological Survey.

Curtis, A., 2014. What percent of volcanoes are glaciated? [WWW document]. Earth science stack exchange. URL. http://earthscience.stackexchange.com/questions/2497/what-percent-of-volcanoes-are-glaciated/2529 (accessed 8.5.16).

Curtis, A., 2015. Dynamics and global relevance of fumarolic ice caves on Erebus Volcano, Antarctica. (PhD Dissertation). Earth and Environmental Science. New Mexico Institute of Mining and Technology.

Curtis, A., Kyle, P., 2011. Geothermal point sources identified in a fumarolic ice cave on Erebus volcano, Antarctica using fiber optic distributed temperature sensing. Geophys. Res. Lett. 38, L16802. http://dx.doi.org/10.1029/2011GL048272.

Edwards, B.R., Russell, J.K., Simpson, K., 2010. Volcanology and petrology of Mathews Tuya, northern British Columbia, Canada: glaciovolcanic constraints on interpretations of the 0.730 Ma Cordilleran paleoclimate. Bull. Volcanol. 73:479–496. http://dx.doi.org/10.1007/s00445-010-0418-z.

Edwards, B., Magnússon, E., Thordarson, T., Guðmundsson, M.T., Höskuldsson, A., Oddsson, B., Haklar, J., 2012. Interactions between lava and snow/ice during the 2010 Fimmvörðuháls eruption, south-central Iceland. J. Geophys. Res. 117, B04302. http://dx.doi.org/10.1029/2011JB008985.

Edwards, B.R., Belousov, A., Belousova, M., 2014. Propagation style controls lava–snow interactions. Nat. Commun. 5:5666. http://dx.doi.org/10.1038/ncomms6666.

Global Volcanism Program, 2013. Volcanoes of the World, v. 4.5.0 http://dx.doi.org/10.5479/si.GVP.VOTW4-2013.

Global Volcanism Program, 2016. Report on Cotopaxi (Ecuador). In: Sennert, S.K. (Ed.), Weekly Volcanic Activity Report.

Grapenthin, R., Freymueller, J.T., Kaufman, A.M., 2013. Geodetic observations during the 2009 eruption of Redoubt Volcano, Alaska. J. Volcanol. Geotherm. Res. 259:115–132. http://dx.doi.org/10.1016/j.jvolgeores.2012.04.021.

Gruber, S., 2012. Derivation and analysis of a high-resolution estimate of global permafrost zonation. Cryosphere 6:221. http://dx.doi.org/10.5194/tc-6-221-2012.

Hall, D.K., Riggs, G.A., 2007. Accuracy assessment of the MODIS snow products. Hydrol. Process. 21:1534–1547. http://dx.doi.org/10.1002/hyp.6715.

Hall, D.K., Salomonson, V.V., Riggs, G.A., 2006. MODIS/Terra Snow Cover Daily L3 Global 500 m Grid V0005. National Snow and Ice Data Center, Boulder, CO USA.

Head, J.W., Wilson, L., 2007. Heat transfer in volcano–ice interactions on Mars: synthesis of environments and implications for processes and landforms. Ann. Glaciol. 45:1–13. http://dx.doi.org/10.3189/172756407782282570.

Huybers, P., Langmuir, C., 2009. Feedback between deglaciation, volcanism, and atmospheric CO_2. Earth Planet. Sci. Lett. 286:479–491. http://dx.doi.org/10.1016/j.epsl.2009.07.014.

Smithsonian Institution, 2013. Global volcanism program | data criteria [WWW document]. URL. http://volcano.si.edu/data_criteria.cfm (accessed 8.5.16).

Keys, J.R., McIntosh, W.C., Kyle, P.R., 1983. Volcanic activity of Mount Melbourne, Northern Victoria Land. Antarct. J. US 18, 10–11.

Kiver, E.P., 1978. Mount Baker's changing fumaroles. Ore Bin 40, 133–145.

Landis, J.R., Koch, G.G., 1977. The measurement of observer agreement for categorical data. Biometrics 33:159–174. http://dx.doi.org/10.2307/2529310.

Major, J.J., Newhall, C.G., 1989. Snow and ice perturbation during historical volcanic eruptions and the formation of lahars and floods. Bull. Volcanol. 52:1–27. http://dx.doi.org/10.1007/BF00641384.

Mazzocchi, M., Hansstein, F., Ragona, M., 2010. The 2010 volcanic ash cloud and its financial impact on the European airline industry. CESifo Forum. Ifo Institute for Economic Research at the University of Munich, pp. 92–100.

Paterson, W.S.B., 1994. The Physics of Glaciers. Butterworth-Heinemann.

Pfeffer, W.T., Arendt, A.A., Bliss, A., Bolch, T., Cogley, J.G., Gardner, A.S., Hagen, J.-O., Hock, R., Kaser, G., Kienholz, C., 2014. The Randolph Glacier inventory: a globally complete inventory of glaciers. J. Glaciol. 60:537–552. http://dx.doi.org/10.3189/2014JoG13J176.

Pierson, T.C., Janda, R.J., Thouret, J.-C., Borrero, C.A., 1990. Perturbation and melting of snow and ice by the 13 November 1985 eruption of Nevado del Ruiz, Colombia, and consequent mobilization, flow and deposition of lahars. J. Volcanol. Geotherm. Res. 41:17–66. http://dx.doi.org/10.1016/0377-0273(90)90082-Q.

Ramon, P., Vallejo, S., Almeida, M., Gomez, J.P., Caceres, B., 2016. Increased melting of Glaciers during Cotopaxi volcano awakening in 2015. EGU General Assembly Conference Abstracts, p. 10769.

Riggs, G.A., Hall, D.K., Salomonson, V.V., 2006. MODIS snow products user guide to collection:5. https://nsidc.org/data/docs/daac/modis_v5/dorothy_snow_doc.pdf.

Sattler, K., Anderson, B., Mackintosh, A., Norton, K., de Róiste, M., 2016. Estimating permafrost distribution in the Maritime Southern Alps, New Zealand, based on climatic conditions at Rock Glacier Sites. Front. Earth Sci. 4. http://dx.doi.org/10.3389/feart.2016.00004.

Schmid, M.-O., Baral, P., Gruber, S., Shahi, S., Shrestha, T., Stumm, D., Wester, P., 2015. Assessment of permafrost distribution maps in the Hindu Kush Himalayan region using rock glaciers mapped in Google Earth. Cryosphere 9:2089–2099. http://dx.doi.org/10.5194/tc-9-2089-2015.

Smellie, J.L., Edwards, B.R., 2016. Glaciovolcanism on Earth and Mars. Cambridge University Press.

Soo, R.M., Wood, S.A., Grzymski, J.J., McDonald, I.R., Cary, C.S., 2009. Microbial biodiversity of thermophilic communities in hot mineral soils of Tramway Ridge, Mount Erebus, Antarctica. Environ. Microbiol. 11:715. http://dx.doi.org/10.1111/j.1462-2920.2009.01859.x.

Tebo, B.M., Davis, R.E., Anitori, R.P., Connell, L.B., Schiffman, P., Staudigel, H., 2015. Microbial communities in dark oligotrophic volcanic ice cave ecosystems of Mt. Erebus, Antarctica. Front. Microbiol. 6. http://dx.doi.org/10.3389/fmicb.2015.00179.

Tolstoy, M., 2015. Mid-ocean ridge eruptions as a climate valve. Geophys. Res. Lett. 42:1346–1351. http://dx.doi.org/10.1002/2014GL063015.

Topf, J., Hormann, C., 2015. Antarctic Icesheet polygons [WWW document]. URL. http://openstreetmapdata.com/data/icesheet-polygons.

Trabant, D., Hawkins, D.B., 1997. Glacier ice volume modeling and glacier volumes on Redoubt Volcano. Alaska: U.S. Geological Survey Water Resources Investigations Report WRI 97-4187 (29 pp.).

Tuffen, H., Castro, J.M., 2009. The emplacement of an obsidian dyke through thin ice: Hrafntinnuhryggur, Krafla Iceland. J. Volcanol. Geotherm. Res. 185:352–366. http://dx.doi.org/10.1016/j.jvolgeores.2008.10.021 (Volcano-Ice Interactions on Earth and Mars: the state of the science).

van Manen, S.M., Dehn, Jonathan, West, M.E., Stephen, Blake, Rothery, D.A., 2010. The 2006 eruption of Augustine Volcano; combined analyses of thermal satellite data and reduced displacement, chapter 23. In: Power, J.A., Coombs, M.L., Freymueller, J.T. (Eds.), The 2006 Eruption of Augustine Volcano, Alaska: U.S. Geological Survey Professional Paper 1769 :pp. 553–567. https://pubs.usgs.gov/pp/1769/chapters/p1769_chapter23.pdf.

Waitt, R.B., Edwards, B.R., Fountain, A.G., 2015. Ice-clad volcanoes. The High-mountain Cryosphere. Cambridge University Press, pp. 272–294.

Wallace, K.L., Neal, C.A., McGimsey, R.G., 2010. Timing, distribution, and character of tephra fall from the 2005–2006 eruption of Augustine Volcano, chapter 9. In: Power, J.A., Coombs, M.L., Freymueller, J.T. (Eds.), The 2006 Eruption of Augustine Volcano, Alaska: U.S. Geological Survey Professional Paper 1769:pp. 187–217 (spreadsheet https://pubs.usgs.gov/pp/1769/chapters/p1769_chapter09).

Wright, R., Blackett, M., Hill-Butler, C., 2015. Some observations regarding the thermal flux from Earth's erupting volcanoes for the period of 2000 to 2014. Geophys. Res. Lett. 42. http://dx.doi.org/10.1002/2014GL061997 (2014GL061997).

Zimbelman, D.R., Rye, R.O., Landis, G.P., 2000. Fumaroles in ice caves on the summit of Mount Rainier—preliminary stable isotope, gas, and geochemical studies. J. Volcanol. Geotherm. Res. 97:457–473. http://dx.doi.org/10.1016/S0377-0273(99)00180-8.